Structural behavior of a polymer chain inside an attractive sphere

Handan Arkın[1,2,*] and Wolfhard Janke[1,†]

[1]*Institut für Theoretische Physik, Universität Leipzig, Postfach 100 920, D-04009 Leipzig, Germany*
[2]*Department of Physics Engineering, Faculty of Engineering, Ankara University, Tandogan, 06100 Ankara, Turkey*

We analyze the structural behavior of a single polymer chain inside an attractive sphere. Our model is composed of a coarse-grained polymer and an attractive-sphere potential. By means of extensive multicanonical Monte Carlo simulations, it is shown that the system exhibits a rich phase diagram ranging from highly ordered compact to extended random coil structures and from desorbed to partially or even completely adsorbed conformations. These findings are identified with different structural observables.

I. INTRODUCTION

The structure formation of polymers and proteins in different environments is crucial for a wide variety of fields in interdisciplinary research and nanotechnological applications. In recent years there have been many applications including, e.g., the fabrication of biosensors [1], peptide adhesion [2] to metals [3,4] and semiconductors [5–7]. Therefore, the understanding of molecular self-assembly near substrates has recently become a fascinating field in an interdisciplinary setting. Within this frame, a deeper knowledge starting from the origin using simplified polymer models is an important subject. Despite many efforts in the past, due to the complexity introduced, for instance, by the huge number of sequence possibilities for proteins and different kinds of environments in general, many problems are still not well understood. The understanding of how the conformational space is affected by the geometric effect that a polymer can experience attraction inside differently shaped cages depends on external parameters such as temperature and attraction strength. The interaction of macromolecules in differently shaped cages is particularly important for the reconstruction of all biological processes such as cellular motion, drug delivery, and enzymatic catalysis. The knowledge of structure formation for a variety of interfaces has therefore been a challenging research field in recent years. It is the prerequisite for designing specifically tailored nanostructures in application of nanotechnology and in different fields such as adhesion, chromatography, biomedical implant modification, and biosensors [8]. It is interesting to understand the mechanism by which proteins and polymers cluster or aggregate on surfaces of different shapes. This provides insight into the growth behavior of polymer layers and thus enables the engineering of bioactive shapes with specific properties.

Our study focuses on a systematic thermodynamic investigation of a polymer–attractive-sphere cage system using Monte Carlo computer simulations. The problem considered in this paper could have practical implications for a broad variety of applications ranging from protein-ligand binding and designing smart sensors to molecular pattern recognition [9–12] and the discovery of new drugs that bind to specific

receptors. Therefore, the theoretical treatment of the adsorption of macromolecules within the framework of minimalistic coarse-grained polymer models in statistical mechanics has been a long-standing problem [13,14] that still attracts a lot of interest [15–25].

The rest of the paper is organized as follows. In Sec. II the model system is described in detail. Then, in Sec. III the multicanonical Monte Carlo simulation method is briefly reviewed and the measured observables are introduced. Section IV presents and discusses the main results for the system under consideration. Finally, Sec. V concludes the paper with a summary of our findings.

II. MODEL

The polymer chain is described by a coarse-grained off-lattice semiflexible model for homopolymers that has also been used for studies of heteropolymers in the frame of the hydrophobic-polar model [26]. As on the lattice, the adjacent monomers are connected by rigid covalent bonds. Thus the distance is kept fixed and set to unity. The contact interaction of lattice models is replaced by a distance-dependent Lennard-Jones (LJ) potential accounting for short-range excluded-volume repulsion and long-range interaction. An additional interaction accounts for the bending energy of any pair of successive bonds. The position vector of the ith monomer, $i = 1, \ldots, N$, is denoted by $\vec{r}_i$. A polymer with N monomers has $N - 1$ bonds of length unity between neighboring monomers and $N - 2$ bending angles ϑ_i, defined through

$$\cos(\vartheta_i) = (\vec{r}_{i+1} - \vec{r}_i) \cdot (\vec{r}_{i+2} - \vec{r}_{i+1}). \tag{1}$$

The LJ potential of nonbonded monomers is of standard 12-6 form. This model was first employed in two dimensions [27] and later generalized to three-dimensional AB proteins [26,28], partially with modifications taking into account implicitly additional torsional energy contributions of each bond. The energy function for the polymer is thus given by

$$E_p = 4 \sum_{i=1}^{N-2} \sum_{j=i+2}^{N} \left(r_{ij}^{-12} - r_{ij}^{-6} \right) + \frac{1}{4} \sum_{i=1}^{N-2} (1 - \cos \vartheta_i). \tag{2}$$

In this work we assume that the polymer chain is confined in an attractive sphere. The interaction of polymer chain

―――――――
*Handan.Arkin@itp.uni-leipzig.de
†Wolfhard.Janke@itp.uni-leipzig.de
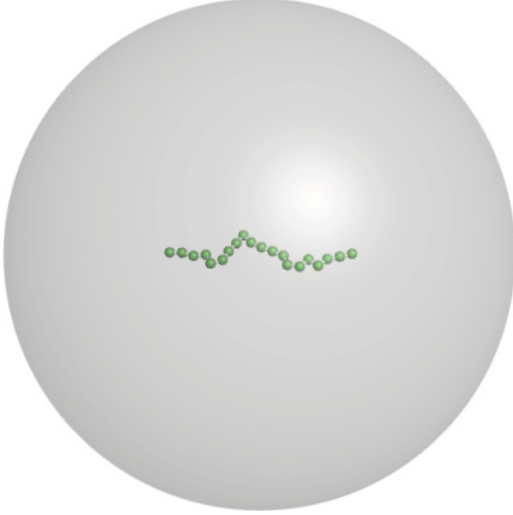
FIG. 1. (Color online) Random start configuration of the simulation. For the sphere radius we choose $R_c = 20$ to let the polymer with $N = 20$ monomers circulate freely inside the sphere.

monomers and the attractive sphere is modeled as

$$
E_s = 4\epsilon_c \frac{\pi R_c}{r_i} \left\{ \frac{1}{5} \left[\left(\frac{\sigma}{R_c - r_i} \right)^{10} - \left(\frac{\sigma}{R_c + r_i} \right)^{10} \right] \right.
$$
$$
\left. - \frac{\epsilon}{2} \left[\left(\frac{\sigma}{R_c - r_i} \right)^4 - \left(\frac{\sigma}{R_c + r_i} \right)^4 \right] \right\}, \qquad (3)
$$

where R_c is the radius of the sphere that is a measure of the cage size, $r_i = (x_i^2 + y_i^2 + z_i^2)^{1/2}$ is the distance of a monomer to the origin, x_i, y_i, z_i are the coordinates of monomers, $\sigma = 1.0$, and $\epsilon_c = 1.0$. For our simulations the polymer chain length is $N = 20$ and we set R_c large enough to enclose the polymer inside the sphere. We also have done simulations with different sizes of the sphere $R_c = 10, 20, 30$. However, to allow the chain to circulate freely inside the sphere and also to reduce the influence on the observables we eventually set it to 20. The parameter ϵ in the second term of Eq. (3) defines the attraction strength of the sphere inner walls and weights the relative importance of intrinsic monomer-monomer and monomer-sphere wall interactions. In our simulations ϵ is varied between 0.1 and 1.2. The total energy $E = E_p + E_s$ of the system is thus composed of the pure polymer chain energy and the polymer–attractive-sphere interaction energy. A start configuration of the simulation is presented in Fig. 1. The initial configuration of the polymer chain is randomly generated where the ends have no contact with the sphere attractive walls. In some theoretical and computational studies the polymer is attached (grafted) at the surface with one of its ends, which reduces the entropic degrees of freedom of the system. However, in many recent experiments of, e.g., peptide-metal or peptide-semiconductor interfaces, the setup of a freely moving polymer is considered. This allows for adsorbed conformations where none of the two polymer ends is in contact with the cage.

III. METHOD

In order to obtain statistical results of sufficient accuracy we applied the multicanonical Monte Carlo algorithm [29] (for reviews, see Refs. [30,31]), where the energy distribution

is flattened artificially, allowing, in principle, for a random walk of successive states in energy space. This flattening is controllable and therefore reproducible. To this end, the Boltzmann probability is multiplied by a weight factor $W(E)$, which in our case is a function of the energy. Then the multicanonical probability for a state $\{\mathbf{x}\}$ with energy $E(\{\mathbf{x}\})$ reads $p_M(E) = \exp(-E/k_B T)W(E)$. In order to obtain a multicanonical or flat distribution, the initially unknown weight function $W(E)$ has to be determined iteratively: In the beginning, the weights $W^{(0)}(E)$ are set to unity for all energies letting the first run be a usual Metropolis simulation, which yields an estimate $H^{(0)}(E)$ for the canonical distribution. This histogram is used to determine the next guess for the weights, the simplest update is to calculate $W^{(1)}(E) = W^{(0)}(E)/H^{(0)}(E)$. Then the next run is performed with probabilities $p_M^{(1)}(E) = \exp(-E/k_B T)W^{(1)}(E)$ of states with energy E, yielding $H^{(1)}(E)$ and $W^{(2)}(E) = W^{(1)}(E)/H^{(1)}(E)$, and so on. The iterative procedure is continued until the weights are appropriate in a way that the multicanonical histogram $H(E)$ is flat. After having determined accurate weights $W(E)$, they are kept fixed and following some thermalization sweeps a long production run is performed, where statistical quantities O are obtained multicanonically, $\langle O \rangle_M = \sum_{\{\mathbf{x}\}} p_M(E(\{\mathbf{x}\}))O(\{\mathbf{x}\})/Z_M$ with the multicanonical partition function $Z_M = \sum_{\{\mathbf{x}\}} p_M(E(\{\mathbf{x}\}))$. The canonical statistics is obtained by reweighting the multicanonical to the canonical distribution, i.e., mean values are computed as $\langle O \rangle = \langle O W^{-1} \rangle_M / \langle W^{-1} \rangle_M$.

For the determination of the multicanonical weights we performed 200 iterations with at least 10^5 sweeps each. In the production period, 1×10^8 sweeps were generated to have reasonable statistics for estimating the thermodynamic quantities. Statistical errors are estimated with the standard jackknife technique [32,33]. As a result, the error bars of the energetic and structural quantities and their fluctuations for $T \geqslant 1.0$ turn out to be smaller than the data symbols used in the plots. For $T \leqslant 1.0$ they are explicitly displayed in the plots of Figs. 2(a), 6(a), and 8(a).

To obtain as much information as possible about the canonical equilibrium behavior, we define the following suitable quantities O. Next to the canonical expectation values $\langle O \rangle$, we also determine the fluctuations about these averages, as represented by the temperature derivative $(\langle OE \rangle - \langle O \rangle \langle E \rangle)/T^2$. We use generic units, in which $k_B = 1$.

In order to identify conformational transitions, the specific heat (per monomer) $C_V(T) = (\langle E^2 \rangle - \langle E \rangle^2)/NT^2$, with $\langle E^k \rangle = \sum_E g(E)E^k \exp(-E/T)/\sum_E g(E)\exp(-E/T)$, is calculated from the density of states $g(E)$. The density of states was found (up to an unimportant overall normalization constant) by reweighting the multicanonical energy distribution obtained with multicanonical sampling to the canonical distribution. Details are given in Ref. [34].

Apart from the specific heat, several structural quantities are of interest. In order to check the structural compactness of conformations or to identify the possible dispersion of conformations because of adsorption, the radius of gyration of the conformations is calculated. The radius of gyration is a measure for the extension of the polymer and defined by $R_g^2 \equiv \sum_{i=1}^{N}(\vec{r}_i - \vec{r}_{\text{c.m.}})^2/N = \sum_{i=1}^{N}\sum_{j=1}^{N}(\vec{r}_i - \vec{r}_j)^2/2N^2$,
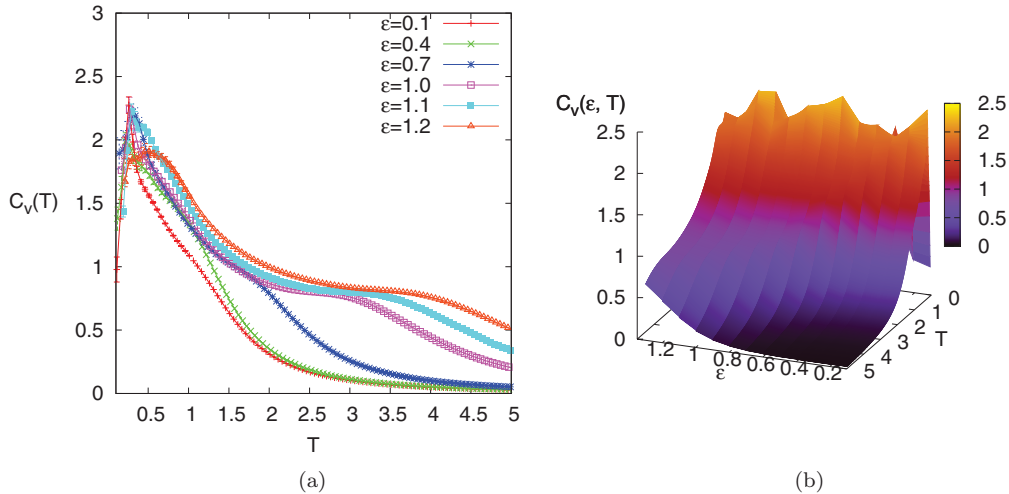
FIG. 2. (Color online) (a) Specific heat as a function of temperature T for selected values of ϵ. (b) Specific heat as a function of the attraction strength ϵ of the inner wall of the sphere and temperature T.

with $\vec{r}_{\text{c.m.}} = \sum_{i=1}^{N} \vec{r}_i / N$ being the center of mass of the polymer.

Another useful quantity is the mean number of monomers docked to the surface. A single-layer structure is formed if all monomers are attached at the sphere; if none is attached, the polymer is desorbed. The sphere potential is a continuous potential and in order to distinguish monomers docked to the sphere inner walls from those not being docked it is reasonable to introduce a cutoff. We define a monomer i as being docked if $R_c - r_i < r_c \equiv 1.2$. The corresponding measured quantity is the average number $\langle N_s \rangle$ of monomers docked to the inner wall. This can be expressed as $N_s = \sum_{i=1}^{N} \Theta(r_c - r_i)$, where $\Theta(r)$ is the Heaviside step function.

IV. RESULTS AND DISCUSSION

Displayed in Fig. 2 are the specific-heat curves $C_V(T)$ as a function of temperature T for different values of ϵ. The specific heat shows two transitions. One is the pronounced low-temperature transition, which is almost at the same temperature for all different ϵ values. This is the freezing transition. Even though this transition occurs at the same temperature, the conformations have different characteristic shapes depending on the attraction strength of the sphere. To describe these different shapes we will concentrate on structural observables to be discussed below. The second, weaker transition signal that can be read off from the specific-heat curves indicates the adsorption transition, which comes into play at higher temperatures than the freezing transition and depends on the sphere attraction strength. This transition separates desorbed (D) and adsorbed (A) conformations. The phase structure derived from the specific-heat curves and supplemented by further information coming from the structural observables is summarized in the pseudophase diagram in the ϵ-T plane of Fig. 3. Representative conformations that predominate in the different structural pseudophases labeled by a letter code adopted from Refs. [22–25] are compiled in Fig. 4.

In the pseudophase diagram the temperature increases from bottom to top and the attraction strength of the sphere inner wall increases from left to right. For low attraction strength, the polymer behaves similarly to a free polymer where below the freezing transition compact conformations [desorbed compact (DC)] are identified and above, globular [desorbed globular (DG)] ones. At higher temperatures a second transition
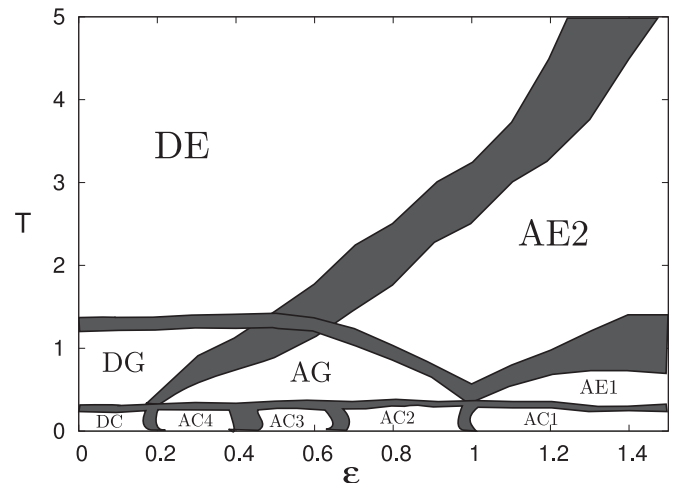
FIG. 3. Phase diagram of the homopolymer–attractive-sphere system as obtained in extensive multicanonical simulations. The boundaries separate the individual conformational phases. The bandwidth shows the variation of the peaks of temperature derivatives of different structural observables that have been analyzed simultaneously. As in the description given in the text, DE, DG, and DC label the desorbed phases of expanded, globular, and crystalline conformations, respectively. In addition, AE1 denotes completely adsorbed and AE2 partially adsorbed expanded structures, AG stands for the adsorbed globular regime, and the crystalline structures occur in various topologies with a different number of layers: AC4, adsorbed spherically symmetric; AC3, adsorbed three-layer structures; AC2, adsorbed two-layer structures; and AC1, adsorbed single-layer structures. Representative conformations are depicted in Fig. 4.
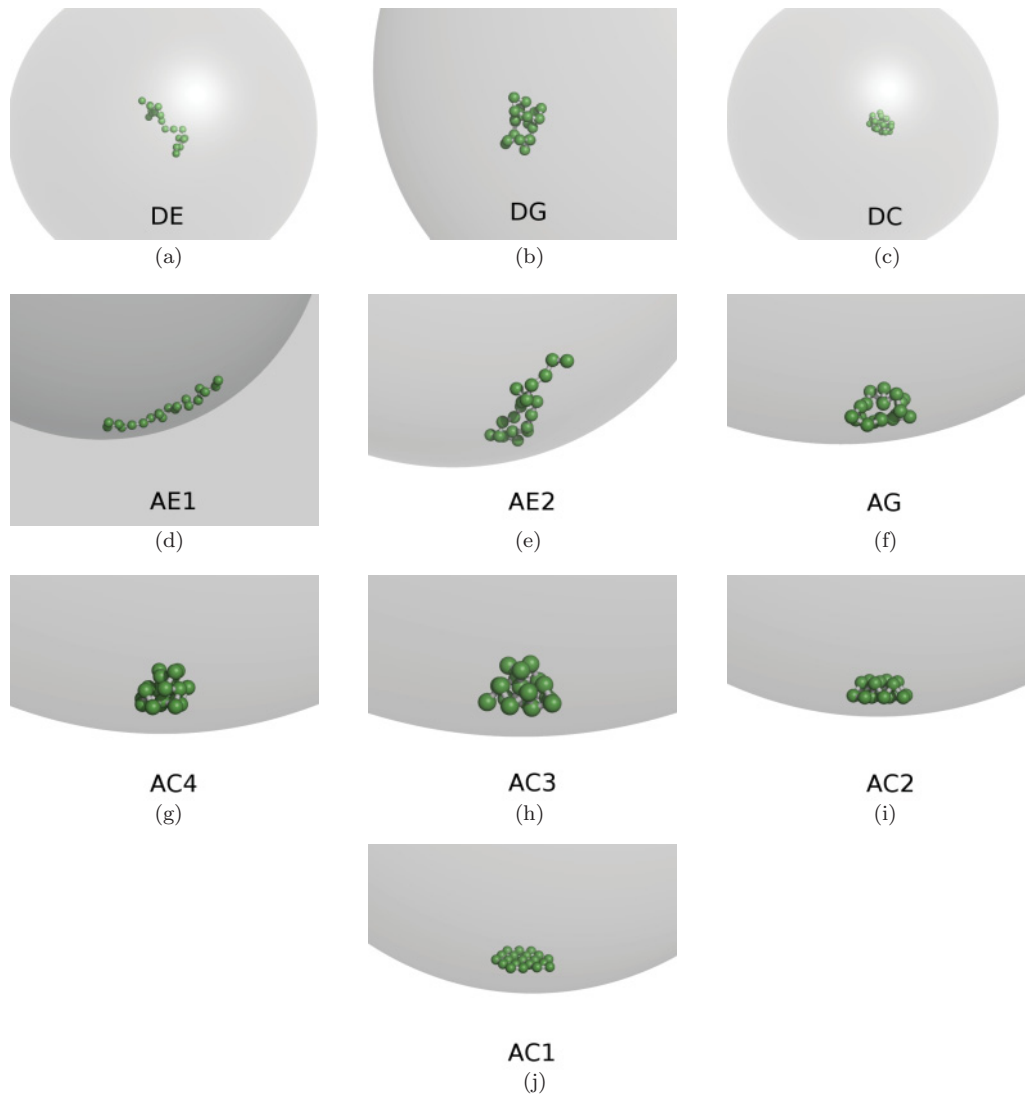
FIG. 4. (Color online) Typical conformations in different regions of the phase diagram: DE, DG, and DC denote the regions where the homopolymer is desorbed; in the other regions labeled by A conformations are adsorbed (for a detailed description see the text).

(in C_V only a shoulder at around $T \approx 1.28$ is visible for low attraction strength) signals the globular to desorbed expanded (DE) or, in other words, random-coil transition. Increasing the attraction strength leads to increasing the temperature of the adsorption transition. The variation of the adsorption transitions depending on the ϵ values can also be nicely seen from the three-dimensional plot of the specific heat that is drawn in Fig. 2(b) as a function of the attraction strength ϵ and temperature T. It is also possible to get an indication from the peaks in Fig. 2(b) at low temperature that occur at $\epsilon \approx 1.0, 0.6$ and a smaller bump at $\epsilon \approx 0.4$. These values correspond to the transitions between the compact pseudophases below the freezing transition.

The radius of gyration parameter provides an excellent view whether the conformations are compact or not; more precisely, we can also get insight into the layering structure of conformations for very high sphere attraction strength. Figure 5 shows the radius of gyration $\langle R_g \rangle$ as a function of temperature for different ϵ values that are considered in our simulations. For small ϵ values $\epsilon = 0.1, 0.2, 0.3, 0.4$, the most

compact conformations occur in the low-temperature region with an average value of $\langle R_g \rangle \approx 1.2$ and the freezing transition temperature is in agreement with that already identified from the specific heat. Additionally, the inflection point of these curves also confirms the temperature that is observed in the specific-heat curve as the collapse transition (random-coil transition). In contrast, slightly increasing the ϵ value causes also an increase in the average $\langle R_g \rangle$ value to about 1.4. Although the freezing transition is hardly affected by the sphere attraction strength, this reveals that there are differently shaped conformations below the freezing transition depending on the sphere attraction strength parameter. Increasing the ϵ parameter further, $\langle R_g \rangle$ jumps to 1.8 at $\epsilon = 1.0$. Above $\epsilon = 1.0$, all other ϵ values yield the typical value $\langle R_g \rangle = 1.8$. From there on we can conclude that the most pronounced transition is the layering transition that occurs at $\epsilon \approx 1.0$ and separates the conformational spaces of planar conformations that are single-layer and totally adsorbed conformations to the sphere inner wall (AC1, AE1) from two-layer (AC2) or three-layer (AC3) and adsorbed spherically compact (AC4) conformations
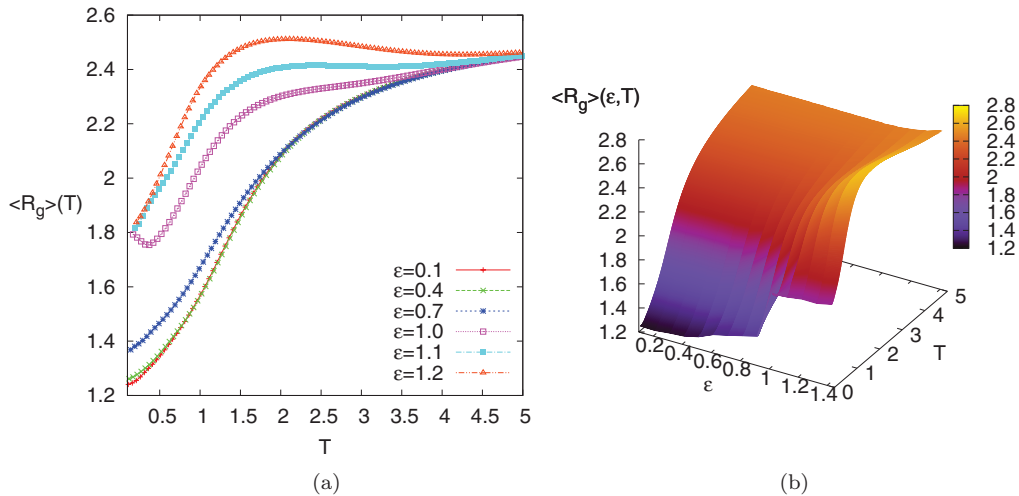
FIG. 5. (Color online) (a) $\langle R_g \rangle$ as a function of temperature T for different values of ϵ. (b) Three-dimensional plot of $\langle R_g \rangle$ as a function of attraction strength ϵ and temperature T.

that are seen at ϵ values lower than $\epsilon \approx 1.0$ and additionally from AG (adsorbed globular), below and above the freezing transition, respectively. This conclusion is also supported by the fluctuations of the radius of gyration $d\langle R_g \rangle/dT$ given in Fig. 6. The biggest deviation in fluctuations occurs at $\epsilon \approx 1.0$ (the three-dimensional figure shows this nicely with a sharp structure in the surface plot for low temperatures). As a result, R_g and its fluctuations establish the transition between DE and DG and between AE2 (adsorbed extended, but not completely adsorbed) and AG and also confirms the freezing transition and the most pronounced layering transitions (signaled by the low-temperature dips at $\epsilon \approx 0.6, 0.4$).

What follows are the low-temperature substructures (AC2, AC3, and AC4) of adsorbed compact conformations. These structures occur when the attraction strength is not yet strong enough to induce one-layer compact structures but sufficiently high to favor polymer-sphere wall contacts. At higher temperature T, two different pictures can be distinguished depending on the competition of chain energy and attraction energy. For low ϵ values the polymer first desorbs (from AG to DG)

and then expands at even higher temperature (from DG to DE). For larger ϵ values the polymer first expands because it is still adsorbed (from AG to AE2) and then at higher temperature desorbs (from AE2 to DE). The AE1 phase occurs for even higher ϵ values. The scenarios are nicely confirmed by the observables and are also revealed by the representative conformations shown in Fig. 4.

Since the adsorption transition typically affects only segments of the polymer and hence is not dominantly signaled by the radius of gyration, we calculated the mean number of monomers docked to the inner wall of the sphere (Fig. 7). Calculating this parameter is the best way to discuss the adsorption transition. As can be seen in Fig. 7(a), for high temperatures and small values of ϵ, the polymer can move freely inside the sphere and the influence of the attractive sphere cannot be seen. Thus the average number of monomer contacts for the value $\epsilon = 0.1$ is like a straight line at $\langle N_s \rangle = 0$. In contrast, for high ϵ values and low temperatures, the polymer has a great tendency to make surface contacts so that the mean number of monomer contacts increases. The first signal of this behavior starts at
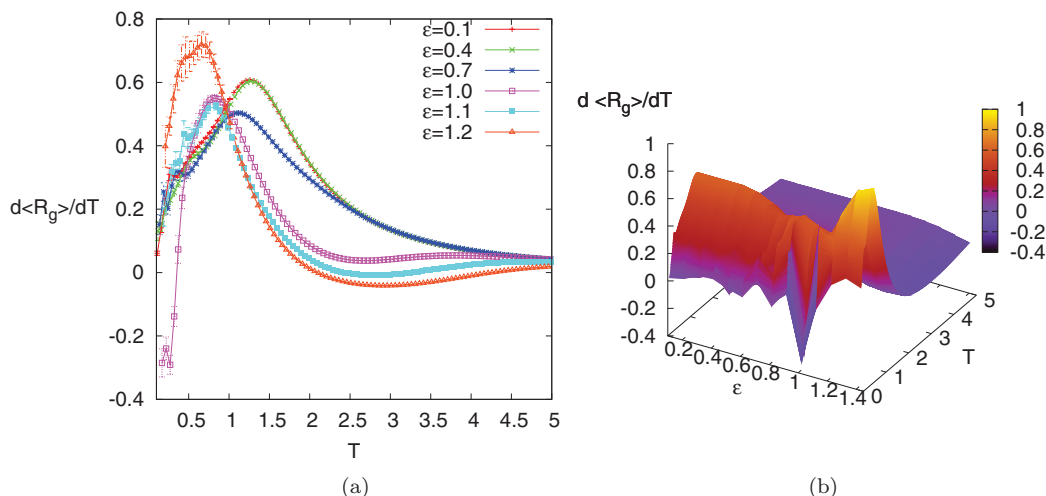
FIG. 6. (Color online) (a) $d\langle R_g \rangle/dT$ for selected values of ϵ and (b) three-dimensional plot of $d\langle R_g \rangle/dT$ plotted against ϵ and T.
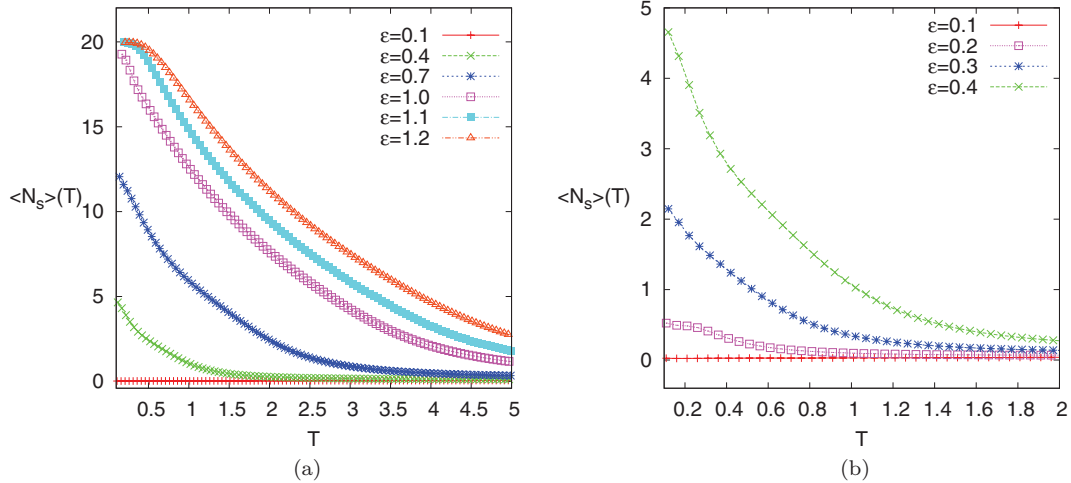
FIG. 7. (Color online) (a) Mean number of adsorbed monomers $\langle N_s \rangle$ at the inner wall of the sphere as a function of temperature T for selected values of ϵ. (b) Magnification of the lower left corner of (a) for small values of ϵ to show the starting point of adsorption, which is $\epsilon \approx 0.2$.

$\epsilon = 0.2$, which can be considered as the adsorption transition [Fig. 7(b)]. For a detailed discussion we can concentrate on the relation $\langle N_s \rangle / N \approx 1/l$ for l-layer structures for lattice polymers [35]. For our three-layer structures this value would be $1/3$. In our simulations where $N = 20$ we found that the three-layer structures observed for $\epsilon = 0.5$ are characterized by $\langle N_s \rangle \geqslant 7.0$. We will discuss this later on when considering the fluctuations of $\langle N_s \rangle$. For the two-layer structures the expected value is $1/2$, which we roughly found for $\epsilon \geqslant 0.7$ as $\langle N_s \rangle \geqslant 10.0$, so that approximately above $\epsilon = 0.7$ two-layer structures are seen below the freezing transition. The reason for some deviation of the numerical values is that most compact multilayer structures are cuboids on the lattice, whereas in our off-lattice study, the layered conformations are semispherical and the lower layer contains more monomers than the upper layers [cf. Figs. 4(g)–4(i)].

Going further to higher ϵ values, at $\epsilon \approx 1.0$, which is also determined from other structural observables as a more pronounced layering transition, the single-layer structures come into play. There the $\langle N_s \rangle$ values are 20 (equal to the chain length) for $\epsilon \geqslant 1.0$. As a result, the most pronounced transition, the single-layer transition, is a topological transition where polymer conformations completely adsorb at the inner wall of the sphere. Also the fluctuations of the mean number of monomer contacts give clear indications of the adsorption transition as well as the layering transition [Figs. 8(a) and 8(b)]. With increasing ϵ the fluctuations of $\langle N_s \rangle$ exhibit three clear deviations that occur at $\epsilon \approx 0.5, 0.7, 1.0$ corresponding to the AC3, AC2, and AC1 (layering transition) structures. In the temperature direction the inflection points give the adsorption transition temperatures, which also depend on the ϵ value.

One more result is illustrated in Fig. 9, where we plot the multicanonical histograms $H(E, R_g)$ for different ϵ values. For $\epsilon = 0.1$ the presence of the most compact conformations (DC) and the others (DG and DE) can be clearly observed. The phase transition from random-coil structures is directed toward globular ones and at low temperature there is only one sharp R_g value. The increase of ϵ leads to some minimal
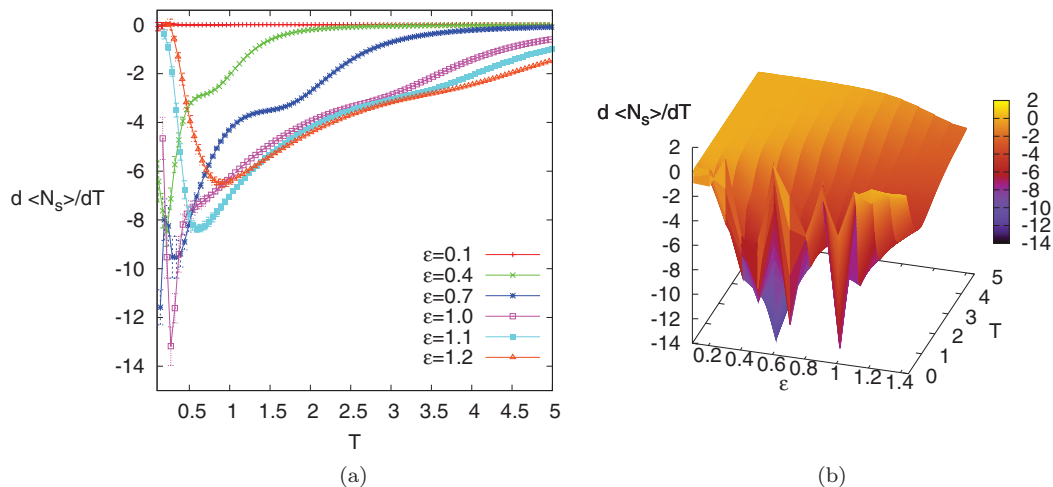
FIG. 8. (Color online) (a) $d\langle N_s \rangle / dT$ for selected values of ϵ and (b) three-dimensional plot of $d\langle N_s \rangle / dT$ plotted against ϵ and T.
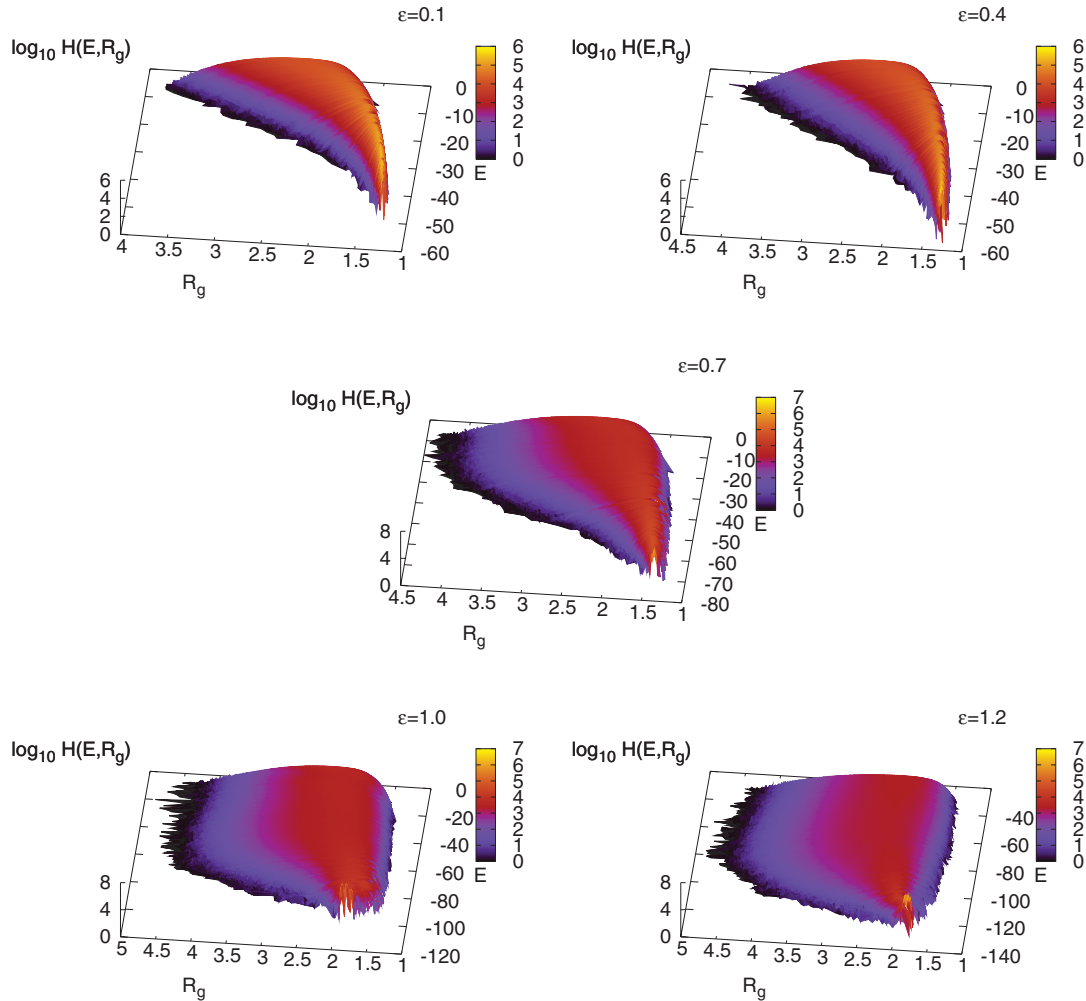
FIG. 9. (Color online) Multicanonical histograms of energy E and radius of gyration R_g for different ϵ values.

change at $\epsilon = 0.4$ because the low-energy part of state space at $\epsilon = 0.4$ is governed by AC4 (adsorbed spherically compact) and AC3 (three-layer) structures, which are also very close to a spherical shape and can be better distinguished by the $\langle N_s \rangle$ parameter indicating the number of adsorbed monomers. Note, however, that the minimum energies are also shifted to much lower energies. This also clearly demonstrates that the polymer sticks to the wall of the sphere. At $\epsilon = 0.7$ the accessible state space broadens while the energies E_p and E_s compete. Additionally, the low-energy part is shifted to higher R_g values. Further increasing ϵ causes more broadening in the conformational space and also more shifting in the R_g values.

All our results obtained from the different observables are summarized by the pseudophase diagram in the ϵ-T plane, which for a convenient overview was already displayed earlier in Fig. 3. Since our system is a finite system, it is not possible to determine the transition lines precisely, but we can clearly identify different pseudophases that show distinguishing features. Their typical conformations were also revealed already in Fig. 4. To summarize these findings, we give a short description of each phase.

Desorbed expanded (DE): Random coil structures with no surface contacts. These conformations freely circulate inside the sphere [Fig. 4(a)].

Desorbed globular (DG): Semicompact disordered conformations. These have also no contacts with the sphere wall [Fig. 4(b)].

Desorbed compact (DC): The compact conformation of the polymer that is not affected by the attractive sphere. Therefore these are desorbed and have no position constraint inside the sphere [Fig. 4(c)].

Adsorbed expanded, single layer (AE1): Completely adsorbed but extended conformations. These are also random-coil-like structures but lie and fit perfectly on the inner wall of the sphere [Fig. 4(d)].

Adsorbed expanded, double layer (AE2): Partially adsorbed, extended conformations. The number of adsorbed monomers depends on how high the attraction strength and temperature are [Fig. 4(e)].

Adsorbed globular (AG): Partially adsorbed, globular conformations like a drop on the inner wall of the sphere [Fig. 4(f)].

Adsorbed compact, spherically shaped (AC4): Partially adsorbed (only one or two monomer-surface contacts) and spherically shaped compact conformations [Fig. 4(g)].

Adsorbed compact, three layer (AC3): Partially adsorbed, compact three-layer conformations. The lower layer of the conformations is adsorbed and lies on the inner wall of the

sphere. The other layers stay on top of them to build up pyramidlike shapes [Fig. 4(h)].

Adsorbed compact, two layer (AC2): Partially adsorbed, compact conformations. These are two-layer structures. The lower layer of the conformations is adsorbed and lies on the inner wall of the sphere [Fig. 4(i)].

Adsorbed compact, single layer (AC1): Completely adsorbed, compact conformations. These single-layer structures lie on the inner wall of the sphere and fit the sphere wall perfectly [Fig. 4(j)].

The transition lines in the pseudophase diagram show the best match of all observables analyzed simultaneously in our study. In the thermodynamic limit of infinitely long chains the transitions are expected to occur at sharp values of the parameters. For finite chains, however, the transition lines still vary with chain length N and are not well defined because of broad peaks in the observables that also have small differences in between. Therefore the locations of the phase boundaries should be considered as a rough guide. Even for the rather short chains considered here, a reasonable picture is obtained and most of the phases are believed to still exist for longer chains. It is clear that the structural behavior of the small chains studied is affected by finite-size effects, in particular in the compact pseudophases. As long as surface effects are as influential as volume effects, the shapes of compact adsorbed (but also of compact desorbed) conformations differ noticeably for polymers with different but small lengths and a precise classification is difficult. However, for longer chains, the DE, DG, and DC phases obviously will survive. Additionally, filmlike (AC1) and semispherical conformations (AC2, AC3, and AC4), as well as surface-attached globular (AG) shapes, will dominate the respective phases. Currently, the simulation of longer chains, aiming at the identification of all conformational subphases and a quantitative analysis in the thermodynamic limit, is too challenging. Thus a more detailed classification within the compact phases for longer chains is left for future work. In spite of this, the pseudophase diagram gives a good overview of the structural behavior of

a polymer chain inside an attractive sphere that is dependent on environmental parameters such as the attraction strength of the sphere wall and temperature.

V. CONCLUSION

In this paper the structural behavior of polymers within the framework of a minimalistic coarse-grained homopolymer model inside an attractive sphere is presented. As the attractive-sphere potential, a Lennard-Jones–type potential between the effective monomers and the sphere wall is assumed. The representative conformations of some structural phases are shown and some structural parameters of the conformations are extracted. Finally, all the results gained from different observables of the polymer–attractive-sphere system that are dependent on the attraction strength and temperature are summarized in the pseudophase diagram, which gives a good overview of the system under consideration. Despite the simplicity of the model, it is possible to see some basic characteristics of structure formation in an attractive sphere. The work considered in this paper could have practical implications for a wide variety of problems ranging from protein-ligand binding to designing smart sensors.

[1] R. F. Service, Science **270**, 230 (1995).

[2] S. Walheim, E. Schaffer, J. Mlynek, and U. Steiner, Science **283**, 520 (1999).

[3] S. Brown, Nature Biotechnol. **15**, 269 (1997).

[4] R. Braun, M. Sarikaya, and K. Schulten, J. Biomater. Sci. Polym. Ed. **13**, 747 (2002).

[5] S. R. Whaley, D. S. English, E. L. Hu, P. F. Barbara, and A. M. Belcher, Nature (London) **405**, 665 (2000).

[6] K. Goede, P. Busch, and M. Grundmann, Nano Lett. **4**, 2115 (2004).

[7] M. Bachmann, K. Goede, A. G. Beck-Sickinger, M. Grundmann, A. Irbäck, and W. Janke, Angew. Chem. Int. Ed. **49**, 9530 (2010).

[8] E. Nakata, T. Nagase, S. Shinkai, and I. Hamachi, J. Am. Chem. Soc. **126**, 490 (2004).

[9] T. Bogner, A. Degenhard, and F. Schmid, Phys. Rev. Lett. **93**, 268108 (2004).

[10] E. Balog, T. Becker, M. Oettl, R. Lechner, R. Daniel, J. Finney, and J. C. Smith, Phys. Rev. Lett. **93**, 028103 (2004).

[11] M. Ikeguchi, J. Ueno, M. Sato, and A. Kidera, Phys. Rev. Lett. **94**, 078102 (2005).

[12] N. Gupta and A. Irbäck, J. Chem. Phys. **120**, 3983 (2004).

[13] E. Eisenriegler, *Polymers near Surfaces* (World Scientific, Singapore, 1993).

[14] G. J. Fleer, M. A. Cohen Stuart, J. M. H. M. Scheutjens, T. Cosgrove, and B. Vincent, *Polymers at Interfaces* (Chapman and Hall, London, 1993).

[15] H. W. Diehl and M. Shpot, Nucl. Phys. B **528**, 595 (1998).

[16] A. Sikorski, Macromol. Theory Simul. **11**, 359 (2002).

[17] M. Bachmann and W. Janke, Phys. Rev. Lett. **95**, 058102 (2005).

[18] M. Bachmann and W. Janke, Phys. Rev. E **73**, 041802 (2006).

[19] M. Bachmann and W. Janke, Phys. Rev. E **73**, 020901(R) (2006).

[20] K. Binder, J. Baschnagel, M. Müller, W. Paul, and F. Rampf, Macromol. Symp. **237**, 128 (2006).

[21] J. Luettmer-Strathmann, F. Rampf, W. Paul, and K. Binder, J. Chem. Phys. **128**, 064903 (2008).

[22] M. Möddel, M. Bachmann, and W. Janke, J. Phys. Chem. B **113**, 3314 (2009).

[23] M. Möddel, W. Janke, and M. Bachmann, Phys. Chem. Chem. Phys. **12**, 11548 (2010).

[24] M. Möddel, W. Janke, and M. Bachmann, Macromolecules **44**, 9013 (2011).

[25] S. Karalus, W. Janke, and M. Bachmann, Phys. Rev. E **84**, 031803 (2011).

[26] A. Irbäck, C. Peterson, F. Potthast, and O. Sommelius, J. Chem. Phys. **107**, 273 (1997).

[27] F. H. Stillinger, T. Head-Gordon, and C. L. Hirshfeld, Phys. Rev. E **48**, 1469 (1993); F. H. Stillinger and T. Head-Gordon, *ibid.* **52**, 2872 (1995).

[28] A. Irbäck, C. Peterson, and F. Potthast, Phys. Rev. E **55**, 860 (1997).

[29] B. A. Berg and T. Neuhaus, Phys. Lett. B **267**, 249 (1991); Phys. Rev. Lett. **68**, 9 (1992); B. A. Berg and T. Çelik, *ibid.* **69**, 2292 (1992); W. Janke, Int. J. Mod. Phys. C **3**, 1137 (1992).

[30] B. A. Berg, Fields Inst. Commun. **26**, 1 (2000).

[31] W. Janke, Physica A **254**, 164 (1998).

[32] B. Efron, *The Jackknife, the Bootstrap and Other Resampling Plans* (Society for Industrial and Applied Mathematics, Philadelphia, 1982).

[33] W. Janke, in *Computational Many-Particle Physics*, edited by H. Fehske, R. Schneider, and A. Weiße, *Proceedings of the Wilhelm & Else Heraeus Summerschool, Greifswald*, Lecture Notes Phys., Vol. 739 (Springer, Berlin, 2008), pp. 79–140.

[34] M. Bachmann, H. Arkın, and W. Janke, Phys. Rev. E **71**, 031906 (2005).

[35] J. Krawczyk, A. L. Owczarek, T. Prellberg, and A. Rechnitzer, Europhys. Lett. **70**, 726 (2005).